

Cite this: *Sustainable Energy Fuels*,  
2024, 8, 5449

# Pressure-swing absorption and desorption behaviours of ammonia in bis(trifluoromethylsulfonyl)amide salts†

Manabu Tokushige, Ryota Fujisawa and Junichi Ryu \*

The absorption and desorption behaviours of  $\text{NH}_3$  in bis(trifluoromethylsulfonyl)amide (TFSA) salts were investigated using the pressure-swing method. The effects of cation species and temperature on the  $\text{NH}_3$  absorption behaviour of four TFSA salts, namely,  $\text{Na}[\text{TFSA}]$ ,  $\text{K}[\text{TFSA}]$ ,  $\text{Mg}[\text{TFSA}]_2$ , and  $\text{Ca}[\text{TFSA}]_2$ , were evaluated.  $\text{NH}_3$  was absorbed by these solid TFSA salts, and high  $\text{NH}_3$  desorption was observed for  $\text{Na}[\text{TFSA}]$  at 473 K and  $\text{K}[\text{TFSA}]$  at 300 K. The  $\text{NH}_3$  absorption behaviour varied with the cation of the TFSA salt. Crystallographic refinement showed that the crystal lattice of  $\text{Na}[\text{TFSA}]$  expanded and contracted along the *c*-axis upon  $\text{NH}_3$  absorption and desorption, respectively, indicating the coordination of  $\text{NH}_3$  molecules with cation sites between the lattice layers. For the alkaline-earth metal TFSA salts,  $\text{NH}_4[\text{TFSA}]$  and amide compounds ( $\text{Mg}(\text{NH}_2)_2$  or  $\text{Ca}(\text{NH}_2)_2$ ) were formed after  $\text{NH}_3$  absorption. Therefore, two absorption processes—coordination and dissociation of  $\text{NH}_3$ —occurred in the TFSA salts.

Received 20th June 2024  
Accepted 9th October 2024

DOI: 10.1039/d4se00820k

rsc.li/sustainable-energy

## 1 Introduction

For over a century, ammonia ( $\text{NH}_3$ ) has been produced, addressing food security as a nitrogen-based fertilizer and securing our livelihood by serving as a feedstock for various chemical products.<sup>1,2</sup> However, conventional production (*via* the Haber–Bosch process) requires a substantial amount of energy because of the requirement of high pressures (5–20 MPa) and temperatures ranging from 673 to 873 K for the synthesis of  $\text{NH}_3$ .<sup>1–7</sup> In contrast, Aika *et al.*<sup>8–11</sup> proposed an  $\text{NH}_3$  production system using a Ru catalyst and selective  $\text{NH}_3$  absorber. Conventional separations of  $\text{NH}_3$  involve cryogenic condensation below 240 K,<sup>12–14</sup> even though  $\text{NH}_3$  is obtained from the synthetic reactors at high temperatures ( $\sim 473$  K).<sup>15,16</sup> The cryogenic condensation of high-temperature gases containing  $\text{NH}_3$  and reactants ( $\text{H}_2$  and  $\text{N}_2$ ) requires a substantial amount of energy, and the subsequent reheating to return the reactant gases to the synthetic reactor results in energy loss.<sup>10,11,17–19</sup> The selective  $\text{NH}_3$  absorber reduces energy losses during  $\text{NH}_3$  separation, and swift  $\text{NH}_3$  separation using absorbers enables the synthesis of  $\text{NH}_3$  under mild conditions such as lower pressures and temperatures because the production rate of  $\text{NH}_3$  is improved by the prompt circulation of reactant gases.<sup>11,17–23</sup> Liu and Aika<sup>18–20</sup> confirmed that mixed halide compounds such as  $\text{CaCl}_2$  and  $\text{CaBr}_2$  exhibited a high  $\text{NH}_3$  storage capacity and established the production system for  $\text{NH}_3$  using these

absorbers (the absorber-enhanced Haber–Bosch process). Malmali *et al.*<sup>24–31</sup> demonstrated that  $\text{NH}_3$  was economically and efficiently produced using the absorber-enhanced Haber–Bosch process. They separated  $\text{NH}_3$  using halides as the absorber at 453 K and 0.6 MPa and confirmed that the production of  $\text{NH}_3$  was determined by the circulation rate of reactant gases. The absorber-enhanced Haber–Bosch process reduces the cost and energy consumption required to produce  $\text{NH}_3$ . Although various types of absorbers have been investigated,<sup>17–41</sup> the operation of the absorber-enhanced Haber–Bosch process has still not been optimized because of the complex  $\text{NH}_3$  absorption and desorption mechanisms, such as the discrete stoichiometry of ammine compounds and slow  $\text{NH}_3$  desorption.<sup>37</sup>  $\text{NH}_3$  is absorbed into halides through the coordination of  $\text{NH}_3$  with the cation and formation of ammine complexes. Subsequently, it desorbs from halides by dissociation of ammine complexes and diffusion of  $\text{NH}_3$  into the gas phase.<sup>19</sup> The formation and dissociation of ammine complexes are relatively slow. The rates of formation and dissociation of ammine complexes are predominantly determined by the heat of reaction (enthalpy change), which serves as the energy barrier for the absorption and desorption of  $\text{NH}_3$ . The dissociation of many ammine compounds requires a substantial heat of reaction ( $\sim 100$  kJ mol<sup>−1</sup>) (Table 1), resulting in a low  $\text{NH}_3$  desorption rate. This implies that the rate and efficiency of  $\text{NH}_3$  production are enhanced by improving the  $\text{NH}_3$  desorption function of the absorber. Malmali *et al.* desorbed  $\text{NH}_3$  from an absorber using the temperature-swing method (TSA). Meanwhile, we have developed a high-temperature  $\text{NH}_3$  absorber to separate  $\text{NH}_3$  obtained at 473 K from the synthetic reactor. This selective absorber reduced the heat loss during cooling and reheating

Graduate School of Engineering, Chiba University, Chiba 263-8522, Japan. E-mail:  
jryu@chiba-u.jp† Electronic supplementary information (ESI) available. See DOI:  
<https://doi.org/10.1039/d4se00820k>

Table 1 NH<sub>3</sub> absorption functions of each absorber at the standard state

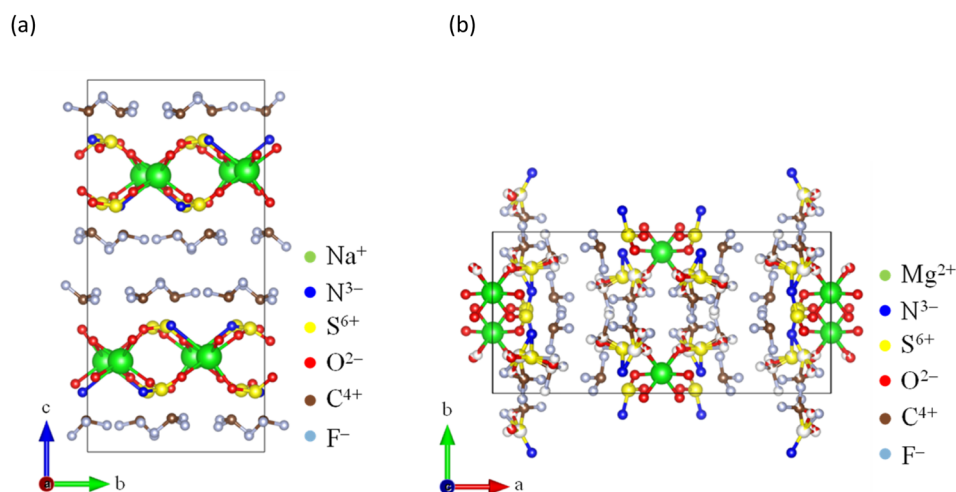
Absorber	Ammine compounds	Storage capacity	Enthalpy change	Reference
MgCl <sub>2</sub>	Mg(NH <sub>3</sub> )Cl <sub>2</sub>	11 mmol g <sup>-1</sup>	-93 kJ mol <sup>-1</sup>	32
	Mg(NH <sub>3</sub> ) <sub>2</sub> Cl <sub>2</sub>	21 mmol g <sup>-1</sup>	-85 kJ mol <sup>-1</sup>	
	Mg(NH <sub>3</sub> ) <sub>6</sub> Cl <sub>2</sub>	63 mmol g <sup>-1</sup>	—	
CaCl <sub>2</sub>	Ca(NH <sub>3</sub> )Cl <sub>2</sub>	9 mmol g <sup>-1</sup>	-81 kJ mol <sup>-1</sup>	
	Ca(NH <sub>3</sub> ) <sub>2</sub> Cl <sub>2</sub>	18 mmol g <sup>-1</sup>	-74 kJ mol <sup>-1</sup>	
	Ca(NH <sub>3</sub> ) <sub>4</sub> Cl <sub>2</sub>	37 mmol g <sup>-1</sup>	-83 kJ mol <sup>-1</sup>	
	Ca(NH <sub>3</sub> ) <sub>8</sub> Cl <sub>2</sub>	72 mmol g <sup>-1</sup>	-164 kJ mol <sup>-1</sup>	
CaBr <sub>2</sub>	Ca(NH <sub>3</sub> )Br <sub>2</sub>	5 mmol g <sup>-1</sup>	-71 kJ mol <sup>-1</sup>	
	Ca(NH <sub>3</sub> ) <sub>2</sub> Br <sub>2</sub>	10 mmol g <sup>-1</sup>	-79 kJ mol <sup>-1</sup>	
	Ca(NH <sub>3</sub> ) <sub>6</sub> Br <sub>2</sub>	20 mmol g <sup>-1</sup>	-182 kJ mol <sup>-1</sup>	
	Ca(NH <sub>3</sub> ) <sub>8</sub> Br <sub>2</sub>	40 mmol g <sup>-1</sup>	-83 kJ mol <sup>-1</sup>	
[emim][TFSA]	—	42 mmol g <sup>-1</sup> @ 1.0 MPa	-7 kJ mol <sup>-1</sup>	33

NH<sub>3</sub> and reactant gases, as NH<sub>3</sub> is easily separated using the pressure-swing method (PSA). Bis(trifluoromethylsulfonyl) amide (TFSA) salts, which are amide salts with imino groups, have several desirable properties such as nonvolatility, nonflammability, high thermal stability, absorption of NH<sub>3</sub>, and low solubilities of H<sub>2</sub> and N<sub>2</sub>.<sup>42–55</sup> For example, NH<sub>3</sub> dissolved in 1-ethyl-3-methyl-imidazolium ([emim]) [TFSA] at 300 K has solubilities of 42.3, 3.36, and 0.527 mmol g<sup>-1</sup> at 1.0, 0.4, and 0.1 MPa, respectively.<sup>33</sup> The heat of dissolution of NH<sub>3</sub> in this TFSA salt (~10 kJ mol<sup>-1</sup>) is lower than that required for the formation of ammine complexes (~100 kJ mol<sup>-1</sup>), which indicates that the rates of absorption and desorption of NH<sub>3</sub> in this TFSA salt are higher than those in halides. Furthermore, TFSA<sup>-</sup> anions can interact with metal centers either as bidentate ligands or by bridging several metal centers.<sup>56</sup> Consequently, alkaline and alkaline-earth metal TFSA salts exhibit layered structures in the solid state, as shown in Fig. 1.<sup>56–59</sup> Because the NH<sub>3</sub> molecule coordinates with a cationic site,<sup>19,23</sup> these solid TFSA salts are expected to absorb NH<sub>3</sub> molecules at each cationic site between the lattice layers. In this study, we

investigated the absorption/desorption behaviour of NH<sub>3</sub> in solid TFSA salts at 473 and 300 K. For four TFSA salts, namely Na[TFSA], K[TFSA], Mg[TFSA]<sub>2</sub>, and Ca[TFSA]<sub>2</sub>, the effects of cation species and temperatures on the NH<sub>3</sub> absorption behaviour were evaluated using crystallographic and kinetic analyses.

## 2 Experimental

The NH<sub>3</sub> absorption/desorption cycles of the four TFSA salts were measured using a magnetic suspension balance (MSB-143, Rubotherm GmbH, Germany) and the pressure-swing method. Commercially available TFSA salts such as Na[TFSA] (purity: >98%; SO989), K[TFSA] (purity: >98%; B2543), Mg[TFSA]<sub>2</sub> (purity: >97%; M2861), and Ca[TFSA]<sub>2</sub> (purity: >97%; C3263) were purchased from Tokyo Chemical Industry Co. Ltd. The experimental setup is described in a separate paper.<sup>60</sup> The TFSA powder sample (~300 mg) was placed in a Pt basket (ø 20 mm × 50 mm) hanging from a magnet, and the basket was suspended inside the furnace *via* the magnetic force. Before initiating the

Fig. 1 Crystal structures of TFSA salts: (a) Na[TFSA]<sup>57</sup> and (b) Mg[TFSA]<sub>2</sub>.<sup>59</sup>

NH<sub>3</sub> absorption/desorption cycle, the TFSA sample was dehydrated at 493 K for 1 h under vacuum as pretreatment. After dehydration, pure NH<sub>3</sub> gas (99.9% purity; Resonac Holdings Corp., Tokyo, Japan) was introduced into the furnace. NH<sub>3</sub> absorption into the sample was conducted under a NH<sub>3</sub> gas pressure of 0.5 MPa for 2 h (pressure-swing absorption), whereas NH<sub>3</sub> desorption was conducted under a NH<sub>3</sub> gas pressure of 0.1 MPa for 3 h (pressure-swing desorption). The pressure of NH<sub>3</sub> was controlled by the temperature of the NH<sub>3</sub> tank immersed in an ethanol bath. After NH<sub>3</sub> absorption/desorption cycles, the sample powders were characterized using X-ray diffraction (XRD; Ultima IV, Rigaku Corp., Japan). XRD data were obtained in the  $2\theta$  range of 5–90° at room temperature, with a step interval of 0.01°, using Cu-K $\alpha$  radiation, calibrated with Si powder. The obtained diffraction patterns were analysed *via* the entire powder pattern fitting method,<sup>61,62</sup> using PDXL (Rigaku Corp.) and split pseudo-Voigt functions. The corresponding crystal structures were visualized using VESTA.<sup>63</sup>

### 3 Results and discussion

#### 3.1 Absorption and desorption behaviours of ammonia

Typical NH<sub>3</sub> absorption/desorption cycles for Na[TFSA] at 473 K are shown in Fig. 2. Na[TFSA] exhibits a stable NH<sub>3</sub> absorption capacity at 473 K and all pressures (0.1 and 0.5 MPa of NH<sub>3</sub> gas). The absorption capacity ( $C_{\text{abs}}$ ) and desorption capacity ( $C_{\text{des}}$ ) of NH<sub>3</sub> are defined as follows:

$$C_{\text{abs}} = \frac{W_{\text{abs}} - W_{\text{s}}}{W_{\text{s}}} \times \frac{1}{M_{\text{NH}_3}} \quad (1)$$

$$C_{\text{des}} = \frac{|W_{\text{des}} - W_{\text{abs}}|}{W_{\text{s}}} \times \frac{1}{M_{\text{NH}_3}} \quad (2)$$

where  $W_{\text{s}}$  is the sample weight before the NH<sub>3</sub> absorption/desorption cycle,  $W_{\text{abs}}$  is the sample weight after the absorption cycle, and  $W_{\text{des}}$  is the sample weight after the desorption cycle.  $M_{\text{NH}_3}$  is the molar weight of NH<sub>3</sub>. The absorption/desorption rates ( $v_{\text{abs}}$  and  $v_{\text{des}}$ ) are defined as the rates at which 80% of the capacity is achieved in each cycle. Na[TFSA] absorbs NH<sub>3</sub> ( $C_{\text{abs}} = 3.05 \text{ mmol g}^{-1}$ ) and exhibits the highest NH<sub>3</sub> desorption capacity ( $C_{\text{des}} = 2.83 \text{ mmol g}^{-1}$ ) among the four TFSA salts. This result indicates that almost all of the

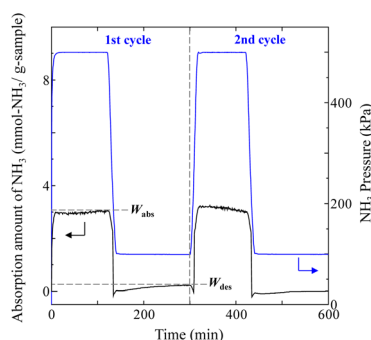


Fig. 2 Typical NH<sub>3</sub> absorption/desorption cycles of Na[TFSA] at 473 K.

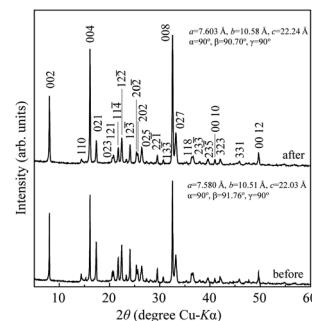
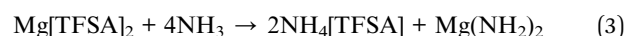


Fig. 3 XRD patterns of Na[TFSA] before and after NH<sub>3</sub> absorption/desorption cycles at 473 K.

absorbed NH<sub>3</sub> in Na[TFSA] can be collected *via* PSA. The XRD patterns of the Na[TFSA] powder before and after the NH<sub>3</sub> absorption/desorption cycles are shown in Fig. 3. The observed diffraction patterns are consistent with Na[TFSA] with a monoclinic  $P21/n$  structure,<sup>57</sup> exhibiting crystal orientation and expansion along the  $c$ -axis after the absorption/desorption cycles. This result suggests that the NH<sub>3</sub> molecules are absorbed between the lattice layers of Na[TFSA]. As shown in Fig. 4, the NH<sub>3</sub> absorption behaviour varies based on the cation species of the TFSA salts. The results of the NH<sub>3</sub> absorption/desorption cycles for each TFSA sample are summarized in Table 2. Only a small amount of NH<sub>3</sub> is absorbed by K[TFSA] (Fig. 4a). Among the TFSA salts, Mg[TFSA]<sub>2</sub> exhibits the highest NH<sub>3</sub> absorption capacity ( $C_{\text{abs}} = 8.29 \text{ mmol g}^{-1}$ ) at 473 K, although the desorption capacity is low ( $C_{\text{des}} = 1.22 \text{ mmol g}^{-1}$ ) (Fig. 4b and Table 2). The  $C_{\text{abs}}$  values increase in the order of Mg[TFSA]<sub>2</sub> > Ca[TFSA]<sub>2</sub> > Na[TFSA]. This result is consistent with that reported by Liu and Aika.<sup>23</sup> They identified the absorption site of NH<sub>3</sub> and clarified the absorption mechanism with alkaline or alkaline-earth metal cations using a thermal conductivity detector and FT-IR spectroscopy. NH<sub>3</sub> is absorbed at these cation sites by three processes: coulombic attraction, the formation of ammonium ions, and the formation of ammine complexes in cation sites. Therefore, it is likely that NH<sub>3</sub> is absorbed at the alkaline or alkaline-earth metal cations of the TFSA salts. Based on the results of Liu and Aika,<sup>23</sup> NH<sub>3</sub> molecules are absorbed through the coulombic attraction between alkaline or alkaline-earth metal cations and the nitrogen anions of NH<sub>3</sub>. Therefore,  $C_{\text{abs}}$  varies with the surface charge density of the alkaline or alkaline-earth metal cations. After the NH<sub>3</sub> absorption/desorption cycle at 473 K, the solid Mg[TFSA]<sub>2</sub> liquefies (Fig. 5b). This liquefaction decreases the NH<sub>3</sub> desorption from Mg[TFSA]<sub>2</sub>. The XRD pattern of the solidified Mg[TFSA]<sub>2</sub> sample at room temperature is shown in Fig. 6a. The observed diffraction pattern is assigned to NH<sub>4</sub>[TFSA] with an orthorhombic  $Pnab$  structure<sup>65</sup> and Mg(NH<sub>2</sub>)<sub>2</sub> with a cubic  $I4_1/acd:2$  structure,<sup>66</sup> indicating that the Mg<sup>2+</sup> cations are displaced by NH<sub>4</sub><sup>+</sup> cations as follows:



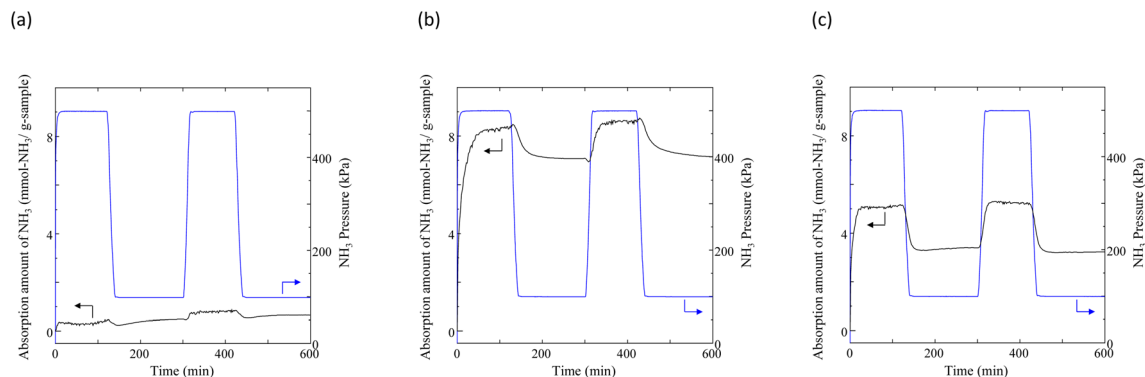


Fig. 4 Typical  $\text{NH}_3$  absorption/desorption cycles for TFSA salts at 473 K: (a)  $\text{K}[\text{TFSA}]$ , (b)  $\text{Mg}[\text{TFSA}]_2$ , and (c)  $\text{Ca}[\text{TFSA}]_2$ .

Table 2  $\text{NH}_3$  absorption/desorption measurements at 473 K

TFSA	Cycle	Absorption capacity, $C_{\text{abs}}$ ( $\text{mmol g}^{-1}$ )	Absorption rate, $v_{\text{abs}}$ ( $\text{mmol g}^{-1} \text{min}^{-1}$ )	Desorption capacity, $C_{\text{des}}$ ( $\text{mmol g}^{-1}$ )	Desorption rate, $v_{\text{des}}$ ( $\text{mmol g}^{-1} \text{min}^{-1}$ )
$\text{Na}[\text{TFSA}]$	1st	3.05	0.81	2.83	0.17
	2nd	3.03	0.19	3.03	0.20
$\text{Mg}[\text{TFSA}]_2$	1st	8.29	0.36	1.22	0.02
	2nd	8.66	—	1.51	0.02
$\text{Ca}[\text{TFSA}]_2$	1st	5.19	0.47	1.74	0.07
	2nd	5.18	0.32	1.95	0.09
Na-Y zeolite <sup>a</sup>	1st	5.08	4.14	2.18	0.10
	2nd	5.45	0.59	2.09	0.09

<sup>a</sup> The results of Na-Y zeolite were referred from ref. 64.

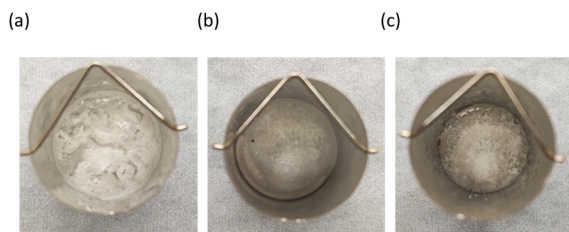


Fig. 5 Photographs of TFSA salts after the  $\text{NH}_3$  absorption/desorption cycles at 473 K: (a)  $\text{Na}[\text{TFSA}]$ , (b)  $\text{Mg}[\text{TFSA}]_2$ , and (c)  $\text{Ca}[\text{TFSA}]_2$  in the Pt basket ( $\varnothing$  20 mm).

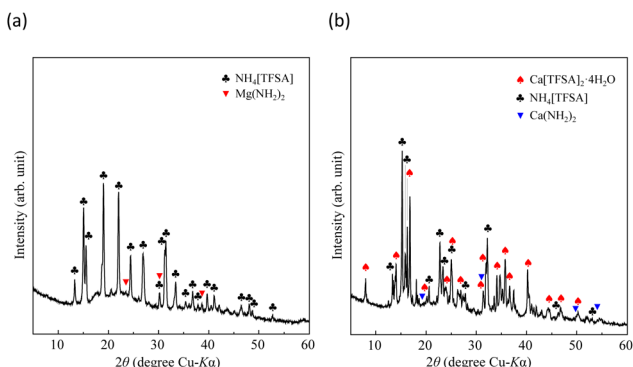


Fig. 6 XRD patterns of alkaline-earth metal TFSA salts after  $\text{NH}_3$  absorption/desorption cycles at 473 K: (a)  $\text{Mg}[\text{TFSA}]_2$  and (b)  $\text{Ca}[\text{TFSA}]_2$ .

Liquefaction of solid salts that absorb excessive  $\text{NH}_3$  has already been reported.<sup>40,60,67</sup> Ammonium ( $\text{NH}_4^+$ ) cations and amide ( $\text{NH}_2^-$ ) anions have been observed in bis(fluorosulfonyl) amide (FSA) salts after  $\text{NH}_3$  absorption, and the FSA salts were liquefied by formation of a eutectic mixture among them.<sup>60</sup> Similarly, the liquefaction of the  $\text{Mg}[\text{TFSA}]_2$  salt can be explained by a eutectic phenomenon. This indicates that the  $\text{NH}_3$  molecule coordinates with the  $\text{Mg}^{2+}$  cation between the lattice layers and dissociates in the  $\text{Mg}[\text{TFSA}]_2$  salt. Therefore, two absorption processes, coordination and dissociation, occur in  $\text{Mg}[\text{TFSA}]_2$ , as shown in Fig. 7. The XRD pattern of the  $\text{Ca}[\text{TFSA}]_2$  sample shows phases of  $\text{Ca}[\text{TFSA}]_2$ ,<sup>57</sup>  $\text{NH}_4[\text{TFSA}]$ , and

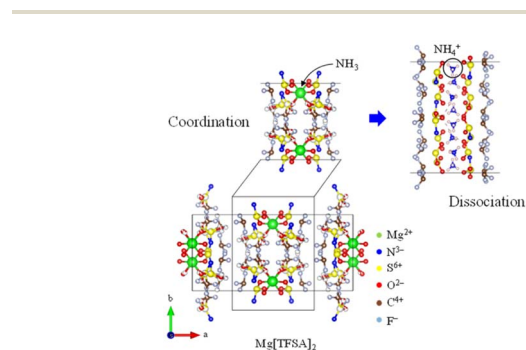


Fig. 7 Absorption mechanism of  $\text{NH}_3$  into TFSA salt.



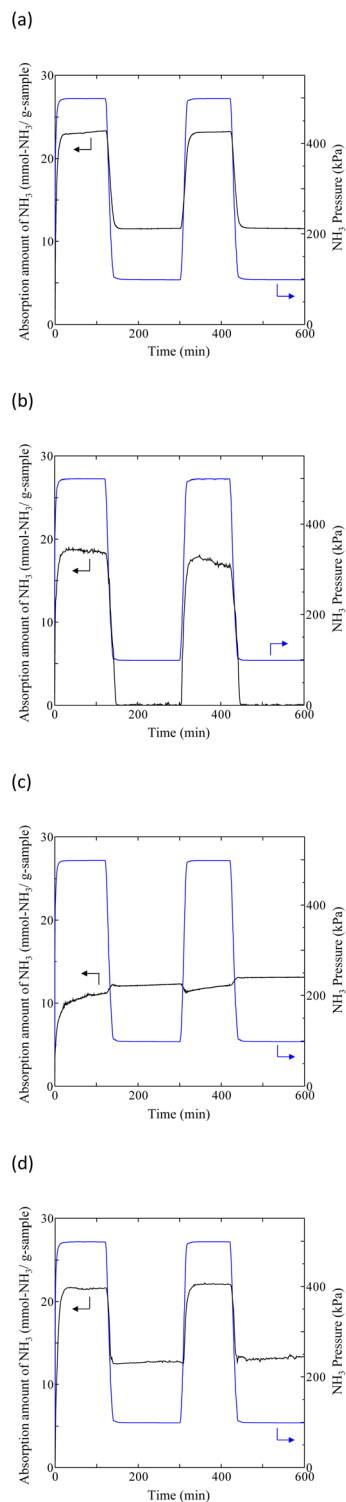


Fig. 8 Typical  $\text{NH}_3$  absorption/desorption cycles in various TFSA salts at 300 K: (a) Na[TFSA], (b) K[TFSA], (c) Mg[TFSA]<sub>2</sub>, and (d) Ca[TFSA]<sub>2</sub>.

$\text{Ca}(\text{NH}_2)_2$  (ref. 68) (Fig. 6b). Therefore, in addition to Mg[TFSA]<sub>2</sub>, the above mentioned two absorption processes occur in Ca[TFSA]<sub>2</sub>. To evaluate the temperature dependence of the  $\text{NH}_3$  absorption/desorption behaviour of the solid TFSA salts,  $\text{NH}_3$

absorption/desorption cycles were examined at 300 K (Fig. 8 and Table 3).  $C_{\text{abs}}$  was higher at lower temperatures. At 300 K, Na[TFSA] exhibited the highest  $C_{\text{abs}}$ . K[TFSA] absorbed  $\text{NH}_3$  under 0.5 MPa and showed the high desorption function of  $\text{NH}_3$ . All absorbed  $\text{NH}_3$  was desorbed from K[TFSA] under 0.1 MPa. The difference of  $\text{NH}_3$  absorption behaviours by temperature can be attributed to the  $\text{NH}_3$  molecular motion. The  $\text{NH}_3$  molecular motion was vigorous and  $C_{\text{abs}}$  decreased at high temperature (473 K). On the other hand, the absorbed  $\text{NH}_3$  did not desorb from Mg[TFSA]<sub>2</sub> at 300 K (Fig. 8b). The crystal lattice of Na[TFSA] shrank after  $\text{NH}_3$  absorption/desorption cycles at 300 K (Fig. 10a), implying that the Na[TFSA] lattice expanded during  $\text{NH}_3$  absorption and shrank during  $\text{NH}_3$  desorption. Mg[TFSA]<sub>2</sub> remained in the solid state after  $\text{NH}_3$  absorption/desorption cycles at 300 K (Fig. 9). The XRD pattern of the Mg[TFSA]<sub>2</sub> sample after cycling at 300 K showed both Mg[TFSA]<sub>2</sub> and  $\text{NH}_4$ [TFSA] phases (Fig. 10b). The  $\text{Mg}^{2+}$  cations in Mg[TFSA]<sub>2</sub> were not entirely displaced by  $\text{NH}_4^+$  cations. Therefore, the absorption process was limited by the dissociation of  $\text{NH}_3$  in Mg[TFSA]<sub>2</sub> at 300 K. Regarding kinetics, the  $\text{NH}_3$  absorption rate of Na[TFSA] was similar to its  $\text{NH}_3$  desorption rate. Na[TFSA] exhibited the highest  $v_{\text{abs}}$  and  $v_{\text{des}}$  among the TFSA samples.  $v_{\text{abs}}$  and  $v_{\text{des}}$  values were higher at lower temperatures. In addition, although all TFSA salts except K[TFSA] showed similar  $\text{NH}_3$  absorption behaviour at 473 K, they exhibited different behaviours at 300 K (Fig. 11). This was caused by the difference in the absorption processes; the absorption into the TFSA salts was limited by the dissociation of  $\text{NH}_3$  in the salts. The double exponential model used to evaluate the kinetics of the two absorption processes is as follows:<sup>69–71</sup>

$$W(t) = A_{\text{crd}} \exp(-k_{\text{crd}}t) + A_{\text{dis}} \exp(-k_{\text{dis}}t) + C \quad (4)$$

where  $W(t)$  is the change in sample weight over time  $t$  after the start of  $\text{NH}_3$  absorption, and  $k_{\text{crd}}$  and  $k_{\text{dis}}$  are the rate constants for the coordination and dissociation of  $\text{NH}_3$ , respectively.

$A_{\text{crd}}$  and  $A_{\text{dis}}$  are the frequency factors for the coordination and dissociation, respectively, and  $C$  is a constant. The first and second terms on the right side of eqn (4) correspond to the coordination and dissociation of  $\text{NH}_3$  in the TFSA salts, respectively. The kinetic parameters were obtained by fitting the initial stage of the  $\text{NH}_3$  absorption curves for each TFSA salt (Fig. 11a and c) using eqn (4), and the values are listed in Tables 4 and 5. The least-squares fitting results are shown in Fig. S1 and S2.† The rate constants of the coordination step are considerably higher than those of the dissociation step ( $k_{\text{crd}} > k_{\text{dis}}$ ), confirming dissociation to be the rate-determining step. The value of  $k_{\text{crd}}$  increases and that of  $k_{\text{dis}}$  decreases with decreasing temperature. For Ca[TFSA]<sub>2</sub> at 300 K,  $k_{\text{dis}}$  is significantly small, suggesting that the dissociation of  $\text{NH}_3$  in Ca[TFSA]<sub>2</sub> is slow at 300 K. Therefore, coordination is the dominant process, whereas dissociation progressed to a lesser extent in the Ca[TFSA]<sub>2</sub> salt.

### 3.2 Comparison of TFSA salts with zeolites

In our previous study,<sup>64</sup>  $\text{NH}_3$  adsorption and desorption behaviours on zeolites at 473 K were observed by PSA cycling



Table 3 NH<sub>3</sub> absorption/desorption measurements at 300 K

TFSA	Cycle	Absorption capacity, $C_{\text{abs}}$ (mmol g <sup>-1</sup> )	Absorption rate, $\nu_{\text{abs}}$ (mmol g <sup>-1</sup> min <sup>-1</sup> )	Desorption capacity, $C_{\text{des}}$ (mmol g <sup>-1</sup> )	Desorption rate, $\nu_{\text{des}}$ (mmol g <sup>-1</sup> min <sup>-1</sup> )
Na[TFSA]	1st	23.34	3.61	11.77	0.53
	2nd	23.26	1.29	11.72	0.52
K[TFSA]	1st	18.48	2.56	18.37	0.63
	2nd	17.02	0.87	17.02	0.60
Ca[TFSA] <sub>2</sub>	1st	21.64	2.05	8.92	0.57
	2nd	22.07	1.25	8.76	0.57

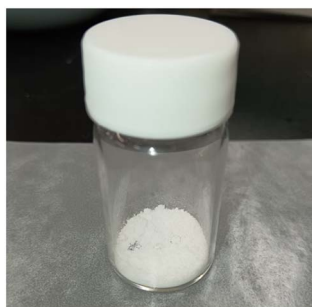


Fig. 9 A photograph of the Mg[TFSA]<sub>2</sub> sample after NH<sub>3</sub> absorption/desorption cycles at 300 K. Mg[TFSA]<sub>2</sub> sample in the glass bottle ( $\varnothing$  24 mm, 10 mL).

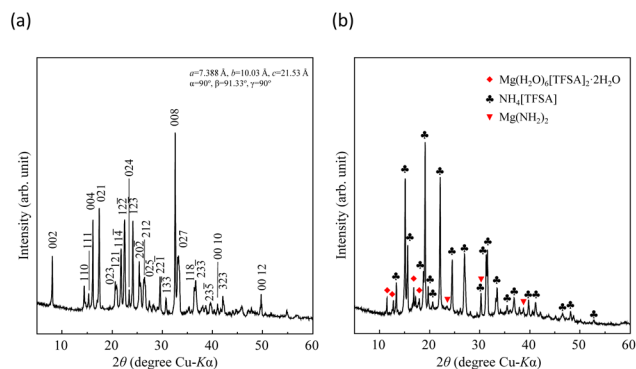


Fig. 10 XRD patterns of TFSA salts after NH<sub>3</sub> absorption/desorption cycles at 300 K: (a) Na[TFSA] and (b) Mg[TFSA]<sub>2</sub>.

(0.1–0.5 MPa), and their stability for NH<sub>3</sub> storage was confirmed. Typical NH<sub>3</sub> adsorption and desorption behaviours of Na–Y and A-4 zeolites at 473 K are shown in Fig. S3.† As shown in Table 2, although the NH<sub>3</sub> adsorption capacity of the Na–Y zeolite ( $C_{\text{ads}} = 5.08$  mmol g<sup>-1</sup>, 7.16 mol m<sup>-3</sup>) is higher than that of Na[TFSA] ( $C_{\text{abs}} = 3.05$  mmol g<sup>-1</sup>, 7.13 mol m<sup>-3</sup>), the NH<sub>3</sub> desorption capacity of the Na–Y zeolite ( $C_{\text{des}} = 2.18$  mmol g<sup>-1</sup>, 3.07 mol m<sup>-3</sup>) is lower than that of Na[TFSA] ( $C_{\text{des}} = 2.83$  mmol g<sup>-1</sup>, 6.62 mol m<sup>-3</sup>). Additionally, the NH<sub>3</sub> desorption rate of Na–Y zeolite ( $\nu_{\text{des}} = 0.10$  mmol g<sup>-1</sup> min<sup>-1</sup>) is lower than that of the Na[TFSA] salt ( $\nu_{\text{des}} = 0.17$  mmol g<sup>-1</sup> min<sup>-1</sup>). Hence, the NH<sub>3</sub> desorption function of the Na–Y zeolite is less than that of Na[TFSA]. These results indicate that zeolites contain non-collectible NH<sub>3</sub> during this PSA cycle (0.1–0.5 MPa, collection ratio: 43%). In contrast, almost all the NH<sub>3</sub> absorbed by the Na [TFSA] salt is collected (collection ratio: 93%). Therefore, the high NH<sub>3</sub> desorption function is an advantage of NH<sub>3</sub> separation using TFSA salts. Finally, to evaluate the durability of the Na[TFSA] for NH<sub>3</sub> absorption/desorption at 473 K, five NH<sub>3</sub> absorption/desorption cycles were conducted (Fig. 12a). Stable NH<sub>3</sub> absorption/desorption behaviours were observed, although the baseline of balance was drifted by multiple changes in NH<sub>3</sub> pressure. From the cycle performance of the NH<sub>3</sub> desorption capacity as a working capacity (Fig. 12b), it was confirmed that Na[TFSA] absorbed and desorbed NH<sub>3</sub> in stably and repeatably. Furthermore, even after five NH<sub>3</sub> absorption/desorption cycles, Na[TFSA] remained as a solid-state and no other compounds such as NH<sub>4</sub>[TFSA] were observed (Fig. 12c). From these results, the durability of the Na[TFSA] was confirmed for NH<sub>3</sub> absorption/desorption at 473 K.

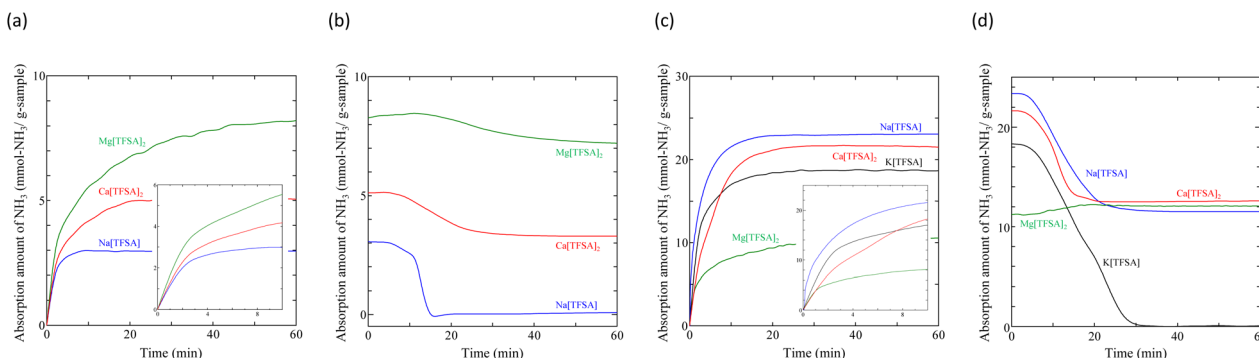


Fig. 11 Initial stages of NH<sub>3</sub> absorption/desorption of TFSA salts: (a) absorption at 473 K, (b) desorption at 473 K, (c) absorption at 300 K, and (d) desorption at 300 K.

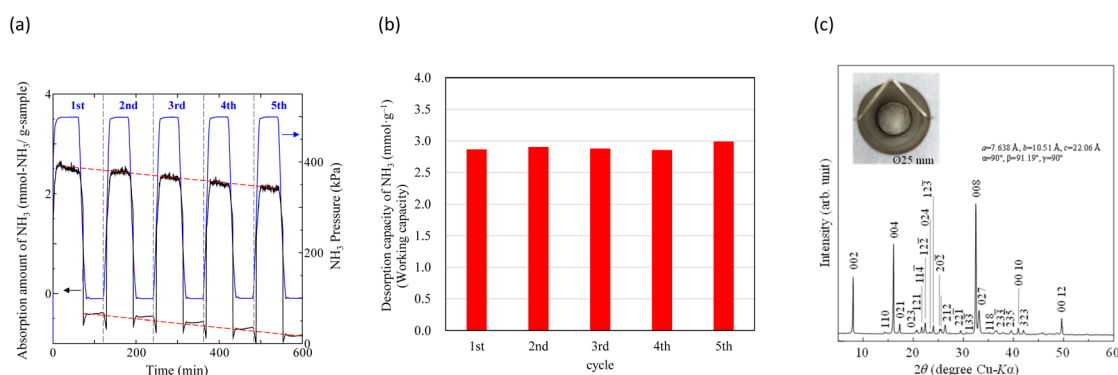


Table 4 Kinetic parameters of NH<sub>3</sub> absorption into TFSA salts at 473 K

TFSA	$A_{\text{erd}}$	$A_{\text{dis}}$	$C$	$k_{\text{erd}} \times 10^{-3} \text{ (s}^{-1}\text{)}$	$k_{\text{dis}} \times 10^{-3} \text{ (s}^{-1}\text{)}$	$R^2$
Na[TFSA]	-2.13927	-2.85738	4.996652	47.22	6.248	0.9994
Mg[TFSA] <sub>2</sub>	-3.44905	-7.41104	10.86009	78.91	2.623	0.9994
Ca[TFSA] <sub>2</sub>	-2.75006	-5.69369	8.44375	62.09	2.520	0.9991

Table 5 Kinetic parameters of NH<sub>3</sub> absorption into TFSA salts at 300 K

TFSA	$A_{\text{erd}}$	$A_{\text{dis}}$	$C$	$k_{\text{erd}} \times 10^{-3} \text{ (s}^{-1}\text{)}$	$k_{\text{dis}} \times 10^{-3} \text{ (s}^{-1}\text{)}$	$R^2$
Na[TFSA]	-10.4859	-27.7007	38.1866	57.22	4.742	0.9999
K[TFSA]	-16.5615	-20.9808	37.5423	19.48	1.188	0.9997
Mg[TFSA] <sub>2</sub>	-7.29562	-9.26933	16.54037	242.0	2.128	0.9967
Ca[TFSA] <sub>2</sub>	-7.03838	-59.9431	66.89941	299.2	0.893	0.9996

Fig. 12 The results of NH<sub>3</sub> absorption/desorption cycles (5 cycles) of Na[TFSA] at 473 K. (a) NH<sub>3</sub> absorption/desorption curves, (b) cycle performance of working capacity, and (c) the XRD pattern of the Na[TFSA] sample after five NH<sub>3</sub> absorption/desorption cycles.

## 4 Conclusions

The NH<sub>3</sub> absorption and desorption behaviours of TFSA salts were investigated using PSA. The effects of the cation species and temperature on the NH<sub>3</sub> absorption behaviour were evaluated for four TFSA salts: Na[TFSA], K[TFSA], Mg[TFSA]<sub>2</sub>, and Ca[TFSA]<sub>2</sub>. NH<sub>3</sub> was absorbed by all of these solid TFSA salts. Among them, Na[TFSA] at 473 K and K[TFSA] at 300 K exhibited high NH<sub>3</sub> desorption ability, with NH<sub>3</sub> desorption capacities of 2.83 and 18.37 mmol g<sup>-1</sup> and collection ratios of 93 and 99%, respectively. The NH<sub>3</sub> absorption behaviour depended on the cation species of the TFSA salt. Crystallographic refinement showed that the crystal lattice of Na[TFSA] expanded and contracted along the *c*-axis during NH<sub>3</sub> absorption and desorption, respectively, suggesting high desorption of NH<sub>3</sub> molecules from the lattice layers. For alkaline-earth metal TFSA salts, NH<sub>4</sub>[TFSA] and amide compounds (Mg(NH<sub>2</sub>)<sub>2</sub> or Ca(NH<sub>2</sub>)<sub>2</sub>) were formed after NH<sub>3</sub> absorption. This indicated that NH<sub>3</sub> dissociated in solid TFSA salts. Therefore, two absorption processes, namely, coordination and dissociation of NH<sub>3</sub>, occurred in the solid TFSA salts. Kinetic analysis confirmed that NH<sub>3</sub> dissociation was the rate-determining step for NH<sub>3</sub> storage in the salts.

## Data availability

The data supporting this article have been included as part of the ESI.†

## Author contributions

M. T.: investigation, data curation, visualization, writing – original draft. R. F.: investigation, data curation. J. R.: supervision, funding acquisition, writing – review and editing, revision and suggestions. All the authors participated in discussions of the results and in preparing the manuscript.

## Conflicts of interest

There are no conflicts to declare.

## Acknowledgements

This research was supported by the Science and Technology Research Partnership for Sustainable Development (SATREPS) in collaboration with the Japan Science and Technology Agency (JST, JPMJSA2104) and the Japan International Cooperation



Agency (JICA). The authors gratefully acknowledge support provided by the Research Foundation. We would also like to thank Mr Shun Mashiko and Mr Morihiro Suzuki for their work on the preliminary experiments.

## References

- J. W. Erisman, M. A. Sutton, J. Galloway, Z. Klimont and W. Winiwarter, *Nat. Geosci.*, 2008, **1**, 636.
- A. Valera-Medina, H. Xiao, M. Owen-Jones, W. I. F. David and P. J. Bowen, *Prog. Energy Combust. Sci.*, 2018, **69**, 63.
- K. E. Lamb, M. D. Dolan and D. F. Kennedy, *Int. J. Hydrogen Energy*, 2019, **44**, 3580.
- D. R. MacFarlane, P.-V. Cherepanov, J. Choi, B. H. R. Suryanto, R. Y. Hodgetts, J. M. Bakker, F. M. F. Vallana and A. N. Simonov, *Joule*, 2020, **4**, 1186.
- M. Ravi and J. W. Makepeace, *Chem. Sci.*, 2022, **13**, 890.
- S. Sun, Q. Jiang, D. Zhao, T. Cao, H. Sha, C. Zhang, H. Song and Z. Da, *Renewable Sustainable Energy Rev.*, 2022, **169**, 112918.
- P. Mayer, A. Ramirez, G. Pezzella, B. Winter, S. M. Sarathy, J. Gascon and A. Bardow, *iScience*, 2023, **26**, 107389.
- K. Aika, H. Hori and A. Ozaki, *J. Catal.*, 1972, **27**, 424.
- K. Aika, *Angew Chem. Int. Ed. Engl.*, 1986, **25**, 558.
- K. Aika and T. Kakegawa, *Catal. Today*, 1991, **10**, 73.
- K. Aika and H. Kobayashi, *CO<sub>2</sub> Free Ammonia as an Energy Carrier*, Springer, Singapore, 2023.
- J. Guo and P. Chen, *Chem*, 2017, **3**, 709.
- Q. Wang, J. Guo and P. Chen, *J. Energy Chem.*, 2019, **36**, 25.
- H. Liu, *Chin. J. Catal.*, 2014, **35**, 1619.
- P. Wang, F. Chang, W. Gao, J. Guo, G. Wu, T. He and P. Chen, *Nat. Chem.*, 2016, **9**, 64.
- R. Shi, X. Zhang, G. I. N. Waterhouse, Y. Zhao and T. Zhang, *Adv. Energy Mater.*, 2020, **10**, 2000659.
- C. Y. Liu and K. Aika, *Chem. Lett.*, 2002, **31**, 798.
- C. Y. Liu and K. Aika, *Ind. Eng. Chem. Res.*, 2004, **43**, 7484.
- C. Y. Liu and K. Aika, *Bull. Chem. Soc. Jpn.*, 2004, **77**, 123.
- C. Y. Liu and K. Aika, *Ind. Eng. Chem. Res.*, 2004, **43**, 6994.
- C. Y. Liu and K. Aika, *Res. Chem. Intermed.*, 2002, **28**, 409.
- C. Y. Liu and K. Aika, *Bull. Chem. Soc. Jpn.*, 2003, **76**, 1463.
- C. Y. Liu and K. Aika, *J. Jpn. Pet. Inst.*, 2003, **46**, 301.
- M. Malmali, Y. Wei, A. McCormick and E. L. Cussler, *Ind. Eng. Chem. Res.*, 2016, **55**, 8922.
- M. Malmali, G. Le, J. Hendrickson, J. Prince, A. V. McCormick and E. L. Cussler, *ACS Sustainable Chem. Eng.*, 2018, **6**, 6536.
- M. Malmali, M. Reese, A. V. McCormick and E. L. Cussler, *ACS Sustainable Chem. Eng.*, 2018, **6**, 827.
- C. Smith, M. Malmali, C. Liu, A. V. McCormick and E. L. Cussler, *ACS Sustainable Chem. Eng.*, 2018, **6**, 11827.
- D. K. Ojha, M. J. Kale, A. V. McCormick, M. Reese, M. Malmali, P. Dauenhauer and E. L. Cussler, *ACS Sustainable Chem. Eng.*, 2019, **7**, 18785.
- B. Lin, T. Wiesner and M. Malmali, *ACS Sustainable Chem. Eng.*, 2020, **8**, 15517.
- B. Lin, F. H. Nowrin, J. J. Rosenthal, A. S. Bhowan and M. Malmali, *ACS Sustainable Chem. Eng.*, 2023, **11**, 9880.
- C. E. Onuoha, M. J. Kale, M. Malmali, P. J. Dauenhauer and A. V. McCormick, *Ind. Eng. Chem. Res.*, 2024, **63**, 5608.
- E. W. Washburn, *International Critical Tables of Numerical Data, Physics, Chemistry and Technology 7*, McGraw-Hill, NY, 1929.
- A. Yokozeki and M. B. Shiflett, *Ind. Eng. Chem. Res.*, 2007, **46**, 1605.
- T. Aoki, T. Ichikawa, H. Miyaoka and Y. Kojima, *J. Phys. Chem. C*, 2014, **118**, 8412.
- Y. Kojima and M. Yamaguchi, *Int. J. Hydrogen Energy*, 2020, **45**, 10233.
- H. Chu, G. Wu, Z. Xiong, J. Guo, T. He and P. Chen, *Chem. Mater.*, 2010, **22**, 6021.
- M. J. Kale, D. K. Ojha, S. Biswas, J. I. Militti, A. V. McCormick, J. H. Schott, P. J. Dauenhauer and E. L. Cussler, *ACS Appl. Energy Mater.*, 2020, **3**, 2576.
- C. Shen, P. Wang, L. Shen, X. Yin and Z. Miao, *Ind. Eng. Chem. Res.*, 2022, **61**, 8616.
- W. Q. Gong, Y. X. Fu, Y. Zhou, M. S. Sun, Z. M. Li, N. H. Lu and D. J. Tao, *Sep. Purif. Technol.*, 2023, **322**, 124304.
- K. Zong and D. Deng, *Sep. Purif. Technol.*, 2024, **349**, 127869.
- Y. Cao, K. Jiang and D. Deng, *Sustainable Energy Fuels*, 2024, **8**, 3933.
- J. Foropoulos and D. D. DesMarteau, *J. Am. Chem. Soc.*, 1982, **104**, 4260.
- J. Foropoulos and D. D. DesMarteau, *J. Fluorine Chem.*, 1982, **21**, 9.
- L. Xue, D. D. DesMarteau and W. T. Pennington, *Angew Chem. Int. Ed. Engl.*, 1997, **36**, 1331.
- P. Johansson, S. P. Gejji, J. Tegenfeldt and J. Lindgren, *Electrochim. Acta*, 1998, **43**, 1375.
- A. Yokozeki and M. B. Shiflett, *Appl. Energy*, 2007, **84**, 1258.
- W. Shi and E. J. Maginn, *AIChE J.*, 2009, **55**, 2414.
- J. Palomar, M. Gonzalez-Miquel, J. Bedia, F. Rodriguez and J. J. Rodriguez, *Sep. Purif. Technol.*, 2011, **82**, 43.
- J. Bedia, J. Palomar, M. Gonzalez-Miquel, F. Rodriguez and J. J. Rodriguez, *Sep. Purif. Technol.*, 2012, **95**, 188.
- Y. Li, M. C. Ali, Q. Yang, Z. Zhang, Z. Bao, B. Su, H. Xing and Q. Ren, *ChemSusChem*, 2017, **10**, 3368.
- F. Zhong, H. Peng, D. Tao, P. Wu, J. Fan and K. Huang, *ACS Sustainable Chem. Eng.*, 2019, **7**, 3258.
- A. Finotello, J. E. Bara, D. Camper and R. D. Noble, *Ind. Eng. Chem. Res.*, 2007, **47**, 3453.
- M. Ramdin, T. W. de Loos and T. J. H. Vlught, *Ind. Eng. Chem. Res.*, 2012, **51**, 8149.
- M. Ramdin, S. P. Balaji, J. M. Vicent-Luna, J. J. Gutiérrez-Sevillano, S. Calero, T. W. de Loos and T. J. H. Vlught, *J. Phys. Chem. C*, 2014, **118**, 23599.
- A. Rivera-Pousa, R. Lois-Cuns, M. Otero-Lema, H. Montes-Campos, T. Méndez-Morales and L. Miguel Varela, *J. Chem. Inf. Model.*, 2024, **64**, 164.
- L. Xue, D. D. DesMarteau and W. T. Pennington, *Solid State Sci.*, 2005, **7**, 311.
- K. Matsumoto, T. Matsui, T. Nohira and R. Hagiwara, *J. Fluorine Chem.*, 2015, **174**, 42.
- L. Xue, C. W. Padgett, D. D. DesMarteau and W. T. Pennington, *Solid State Sci.*, 2002, **4**, 1535.





- 59 G. Veryasov, U. Harinaga, K. Matsumoto and R. Hagiwara, *Eur. J. Inorg. Chem.*, 2017, **2017**, 1087.
- 60 M. Tokushige, R. Fujisawa and J. Ryu, *Sustainable Energy Fuels*, 2024, **8**, 397.
- 61 G. S. Pawley, *J. Appl. Crystallogr.*, 1981, **14**, 357.
- 62 H. Toraya, *J. Appl. Crystallogr.*, 1986, **19**, 440.
- 63 K. Momma and F. Izumi, *J. Appl. Crystallogr.*, 2011, **44**, 1272.
- 64 M. Tokushige and J. Ryu, *ACS Omega*, 2023, **8**, 32536.
- 65 M. G. Davidson, P. R. Raithby, A. L. Johnson and P. D. Bolton, *Eur. J. Inorg. Chem.*, 2003, **2003**, 3445.
- 66 H. Jacobs, *Z. Anorg. Allg. Chem.*, 1971, **382**, 97.
- 67 L. Gao, H. Fang, Z. Li, X. Yu and K. Fan, *Inorg. Chem.*, 2011, **50**, 4301.
- 68 R. Juza and H. Schumacher, *Z. Anorg. Allg. Chem.*, 1963, **324**, 278.
- 69 N. Koga, Y. Goshi, S. Yamada and L. A. Pérez-Maqueda, *J. Therm. Anal. Calorim.*, 2013, **111**, 1463.
- 70 İ. Tosun, *Int. J. Environ. Res. Public Health*, 2012, **9**, 970.
- 71 V. Kiss and K. Ósz, *Int. J. Chem. Kinet.*, 2017, **49**, 602.

